Tellus (1995), 47A, 526–540
Printed in Belgium – all rights reserved

TELLUS
ISSN 0280–6495

Low-frequency variabilities for widely different basic flows

By WILBUR Y. CHEN* and HUUG M. VAN DEN DOOL, *Climate Analysis Center, NOAA/NWS/NMC, 5200 Auth Road, Room 604, Camp Spring, MD 20233, USA*

(Manuscript received 31 August 1994; in final form 10 January 1995)

ABSTRACT

The internal dynamics associated low-frequency variabilities (LFVs) with timescales between 7 days and 31 days, relevant to the potential predictability of monthly means, are investigated. Using observed data and a set of general circulation model produced data, it is shown that the LFV characteristics are distinct for widely different basic flows: much smaller variability for north Pacific cyclonic basic flows than anti-cyclonic basic flows. Their preferred development locations are also distinct. The dynamical processes leading to this large difference is examined in the light of the local barotropic energy conversion between basic flow and low-frequency components. Over the eastern North Pacific where the LFVs are primarily located, the energy conversion decays more from the low-frequency disturbances into the cyclonic basic flows, while much more extraction of LFV energy from the anti-cyclonic basic flows takes place. The internal LFVs considered here are closely related to the climate noise pertaining to the prediction of monthly means. A dynamical link between the phase of El Niño/Southern Oscillation (ENSO) and the potential predictability of monthly means can therefore be established: during the warm phase of ENSO when the mean north Pacific flow is usually cyclonic, the potential predictability of the monthly means can be expected to be higher than during the cool phase, due to the substantially different magnitudes of unpredictable noise being generated through barotropic instability of these different zonally varying basic flows.

1. Introduction

Synoptic-scale eddies are known to barotropically decay into lower-frequency disturbances at the end of their tracks. It is interesting to observe that stronger stormtracks may not necessarily lead to larger lower-frequency variabilities. In this paper, both the observed- and the model-produced lower-frequency variabilities are compared for 2 distinct time-mean flows. Large differences in low-frequency variabilities (LFVs), those disturbances with time-scales between 7 days and 31 days that we are interested in, can be observed. The dynamical nature of the LFV is investigated and the implication of large LFV differences relevant to the prediction of monthly means is assessed.

For widely different zonally-varying basic flows, their inherent barotropic instability should also be different by virtue of their distinct deformation field. It follows that their internal-dynamics-associated variability should also exhibit distinct characteristics. For example, the preferred location for the LFV development and the variance magnitude should all show large differences.

The positive and negative phase of the PNA mode (Wallace and Gutzler, 1981; Barnston and Livezey, 1987) provides perhaps the most prominent difference in zonally varying time-mean flows over the North Pacific, with large positive and large negative deviations of geopotential heights from their climatological values. In order to determine how different the internal dynamics associated LFVs are, we examined the 7- to 31-day timescale fluctuations separately for periods during which the time-mean flows are anomalously large positive (PAC-POS flows), and for periods when they are anomalously large negative (PAC-NEG flows). The results are examined and discussed after a brief description of the data used and the methodology applied.

* Corresponding author.

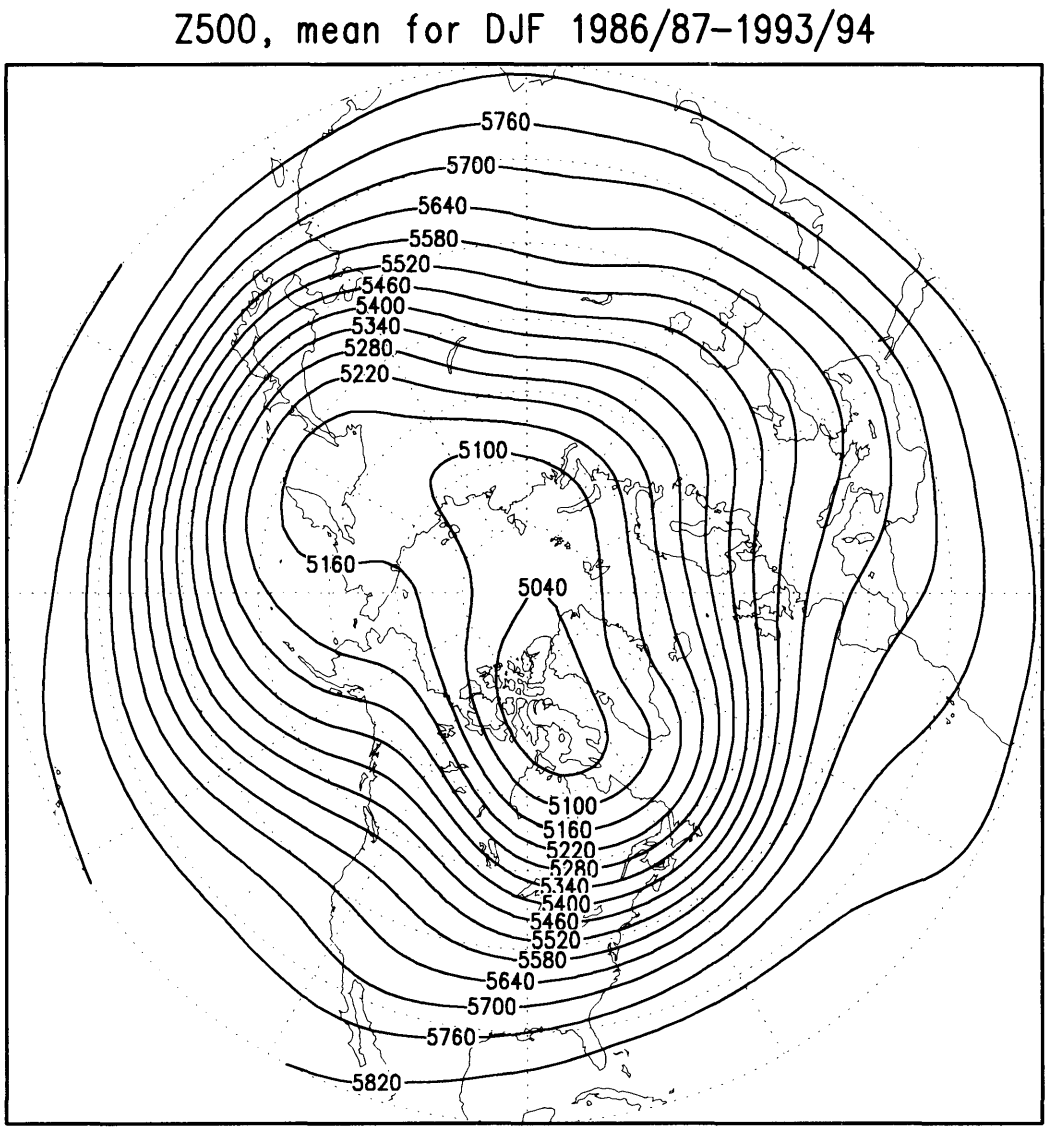

Fig. 1. The DJF mean Z500 for period 1986/87–1993/94. Contour interval is 60 m.

2. Data and methodology

The primary source of data is the NMC-operationally-analyzed geopotential heights and wind fields. Since May 1986, some of the multi-level analyses have been saved by Dr. S. Saha (personal communication). Daily height fields at 500 mb (Z500) and wind fields at 250 mb (U250 and V250) for the last 8 winters (1 November to 31 March, 1986 to 1994) form the primary data set. The Climate Analysis Center also maintains a daily Z500 data set for the last 34 years compiled from the NCAR CD-RAM and the recent NMC analyses (for further detail, see Chen and van den Dool, 1995). This historical record of Z500 is used as a secondary data set to supplement the main part of the present investigation. To further support the observed large differences in LFV for different time-mean flows, general circulation model generated data are also utilized. Further details will be given later in Section 5.

The atmospheric fluctuations we are concerned with in this study are the disturbances with time-scales longer than 7 days and shorter than 31 days, for we are interested in the problem associated with the potential predictability of the monthly means. To obtain the variances of these fluctuations, we simply apply a high-pass filter with n-day running mean on the Z500 time series at each grid point, where n is either 7 days or 31 days. Since the slower variations with time-scale larger than n-days have been filtered out, the high-pass variance, Var(n), is essentially an internal dynamics associated variance, having very little contamination from externally forced variability. Furthermore, since the variance is an additive quantity, we can easily obtain the variance for our LFV by subtracting the estimate of VAR(7) from VAR(31).

The boreal winter time-mean flows were obtained by taking the Z500 time series from 1 November to 31 March and subjecting it first to a 61-day low-pass running mean filter to suppress the shorter timescale fluctuations. The variance of these low-pass filtered time series was then calculated with reference to the 8-winter climatological means. The variance thus obtained contains essentially the interannual variability of the slowly varying time-mean flows. Based on the location of the maximum of this interannual variance, the low-pass filtered time series are then stratified using a threshold level of 50 m. Deviations exceeding +50 m from the climatological values at the variance maximum (47.5° N, 160° W) are collected as the PAC-POS group and those exceeding −50 m are collected as the PAC-NEG group.

3. Basic statistics

Fig. 1 shows the mean Z500 for the DJF season of the last 8 years (1987–1994). This mean Z500 looks like the climatological mean of January obtained by Wallace (1983). It also agrees very closely with the climatologies presented by Blackmon (1976) and Lau et al. (1981). The U250 over the north Pacific is shown in Fig. 2 for the same period. A strong jet with a core speed of over 55 m/s located southeast of Japan and weak

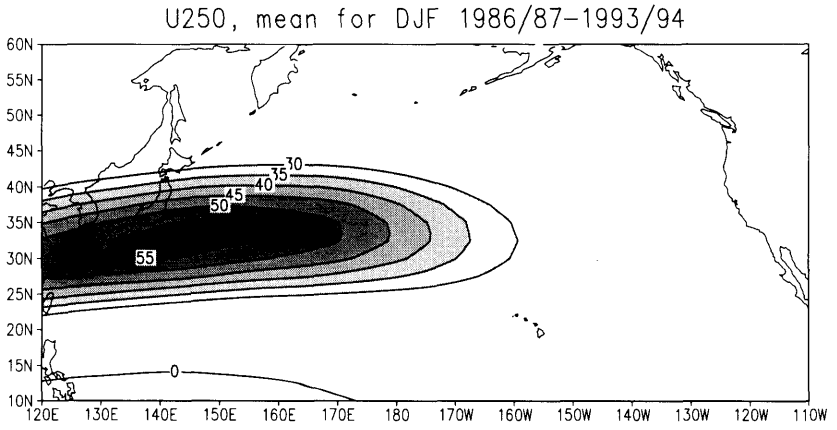

Fig. 2. The DJF mean U250 for period 1986/87–1993/94 (m/s).

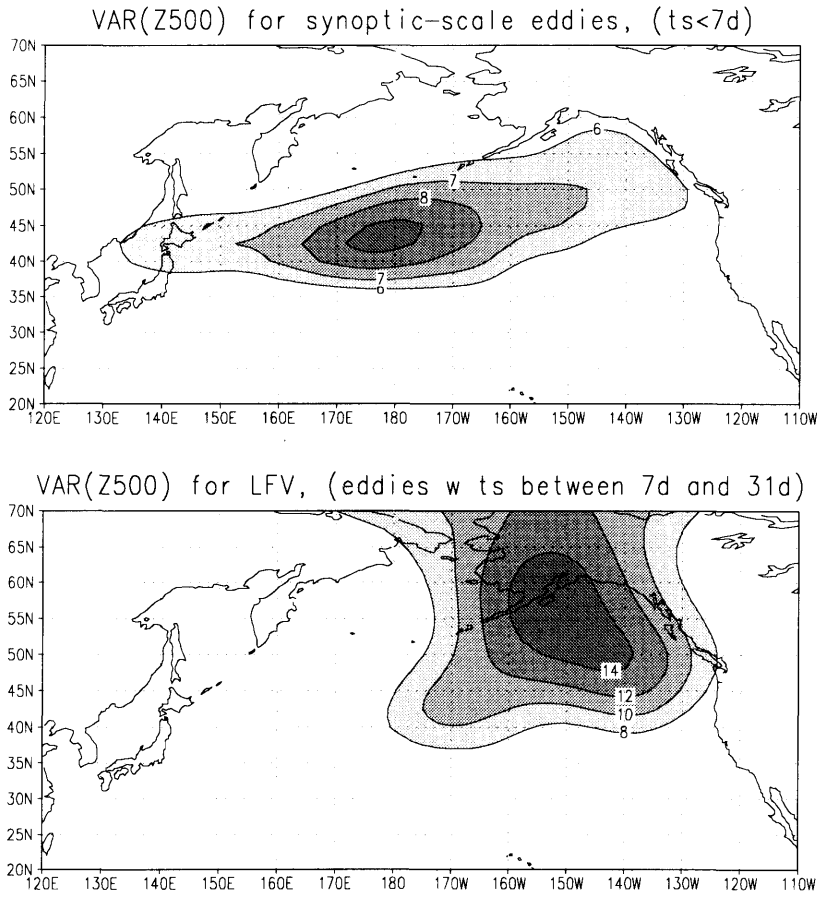

Fig. 3. Internal dynamics associated Z500 variance for (upper panel) synoptic-scale eddies with timescales less than 7 days and (lower panel) low frequency variabilities (LFVs) with timescales longer than 7 days and shorter than 31 days (1000 m^2).

equatorial easterlies south of the jet core are also in good agreement with the above mentioned studies.

The principal north Pacific stormtrack, represented by the large variance of those Z500 fluctuations with time-scale less than 7-days, is shown in the upper panel of Fig. 3, the LFVs in the lower panel. The longitudinally elongated stormtrack and the localized development of the LFV at the end of the track are consistent with the results obtained by the previous authors.

These basic statistics offer us confidence that the 8-winter data, although not as long as we would like to have due to a limited number of upper level wind fields, provide us with sufficient statistically stable results.

4. Stratification

During the last 8 winters, there were periods when the time-mean flows over the North Pacific assumed anomalously large positive or negative deviations from the climatological mean states. We would like to find out, under these drastically different time-mean flow conditions, whether or not their internal-dynamics-associated variabilities exhibit distinct characteristics. For example, do the magnitudes of LFV variance display large differences and do they prefer to develop in different regions of the north Pacific? If they do, what could be the dynamical explanation?

For this purpose, a 61-day running mean low-

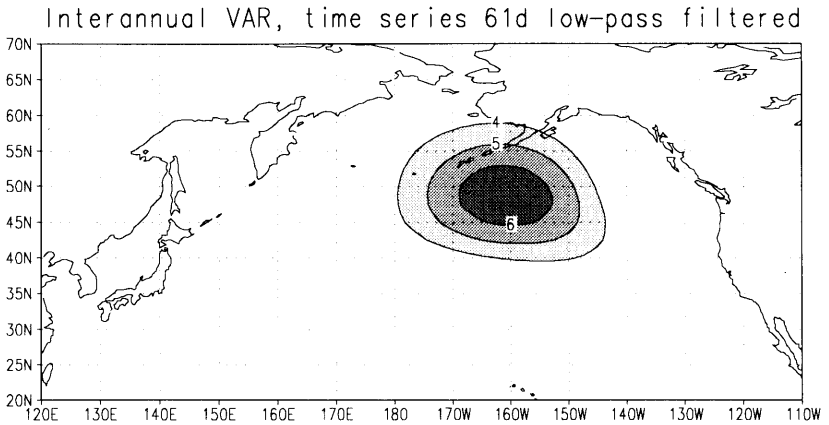

Fig. 4. Interannual Z500 variance for the 61-day low-pass filtered data (1000 m^2).

pass filter was applied to the 8-winter Z500 time-series at each grid point, and the variance with respect to the 8-winter mean of these low-pass filtered time series was obtained and shown in Fig. 4. Contrasting with Fig. 3, the maximum of this interannual variance at grid (47.5° N, 160° W) is located considerably south and west of the maximum of the LFV variance at grid (55° N, 150° W).

Based on this maximum interannual variance at grid point (47.5° N, 160° W), the 61-day low-pass filtered time mean can be stratified into 2 groups, one with a large positive deviation and the other with a large negative deviation from the 8-winter mean climatological state. Two examples are shown as time series in Fig. 5, where the smoothed and heavier solid curve represents the climatological states and the fluctuating lighter solid curve the daily fluctuations of the Z500 heights. The dashed curve is the 61-day low-pass filtered time series. A significant departure of the dashed curve from the heavy solid curve is very apparent. During DJF of 1988/89 (the upper panel, a La Niña northern winter), a large positive shift in the time-mean flow is observed, while a large negative shift is seen during DJF of 1986/87 (the lower panel, an El Niño northern winter).

The PAC-POS (PAC-NEG) group was composed of all days when the 61-day low-pass filtered time series were more than 50 m higher (50 m lower) than the climatological values at grid-point (47.5° N, 160° W). As shown in Fig. 6, the composite circulation patterns look somewhat like the Pacific/North American (PNA) pattern reported

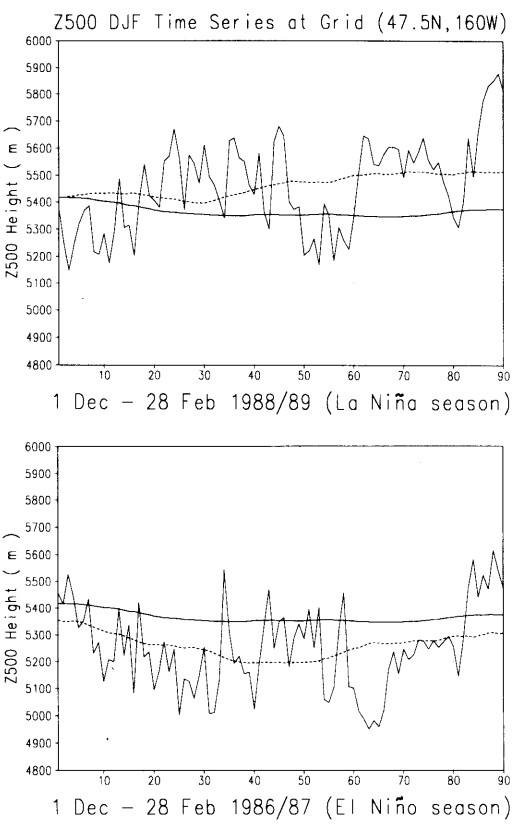

Fig. 5. Time series at grid point (47.5° N, 160° W) for (upper panel) a La Niña season and (lower panel) an El Niño season. The smoothed solid curve is the 8-DJF mean state, the fluctuating solid curve the daily Z500 heights, and the dashed curve the 61-day low-pass filtered time-means.

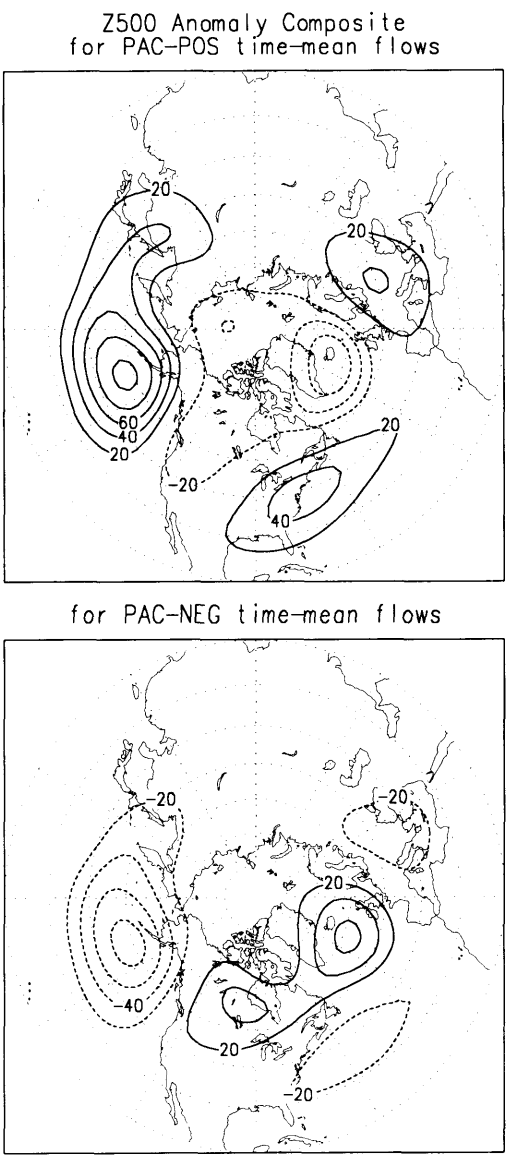

Fig. 6. The Z500 composite anomaly circulation patterns. Solid (dashed) curves for positive (negative) anomalies. PAC-POS (PAC-NEG) stands for Pacific positive (negative) anomaly (m).

by Wallace and Gutzler (1981). Although our PAC-POS and PAC-NEG composites were constructed using only one maximum variance grid point, instead of 4 teleconnection centers of the PNA pattern, we still see the close resemblance between our composites and their PNA pattern. This is not surprising, because during El Niño winters, the North Pacific atmosphere nearly always responds to the tropical anomalous forcing by strengthening the upper level jet and extending it eastward (the lower panel of Fig. 7), resulting in a much stronger cyclonic circulation and a much lower height than the climatological value on the northern flank of the jet. Likewise, during La Niña winters, a much weaker and shorter upper level westerly jet (the upper panel of Fig. 7), results in an anomalously anticyclonic flow and a much higher height than the climatological mean. Therefore, our PAC-NEG (PAC-POS) composite should correspond well with the phase of the PNA mode when its north Pacific center is anomalously below (above) normal.

The north Pacific variances of the synoptic-scale eddies (fluctuations with time-scale less than 7 days) corresponding to PAC-POS and PAC-NEG time-mean flows are shown in Fig. 8. For the PAC-POS flow situations, the stormtrack is diverted northeastward by the anomalous ridge and, at the northeastern flank of the ridge, a secondary track with weaker baroclinic wave activities develops. Under the PAC-NEG time-mean flow conditions, the stormtrack along 45° N extends much further east in association with the eastward extension of the upper level jet (the lower panel of Fig. 8).

The LFV variance, as shown in Fig. 9, develops at the end of each of the principal stormtracks, with locations of maxima substantially different from each other. The LFV variance of the PAC-POS flows are centered over the Alaska/Gulf of Alaska areas, while for the PAC-NEG flows the LFVs are much weaker and centered further south over the eastern North Pacific. What was not quite expected was the much larger LFV variance for the PAC-POS flows than the PAC-NEG flows, more than $(125\ \mathrm{m})^2$ versus about $(100\ \mathrm{m})^2$. Such a large LFV variance difference can not be explained solely by the barotropic decay of synoptic-scale eddies because there is not much difference in the magnitude of the synoptic-scale eddies as shown in Fig. 8.

In order to be sure that the large difference in the LFV variance is not a sampling problem due to limited data set, the LFV variances were also obtained from 31 winters of Z500 historical data (3 of the 34 winters contained long stretches of

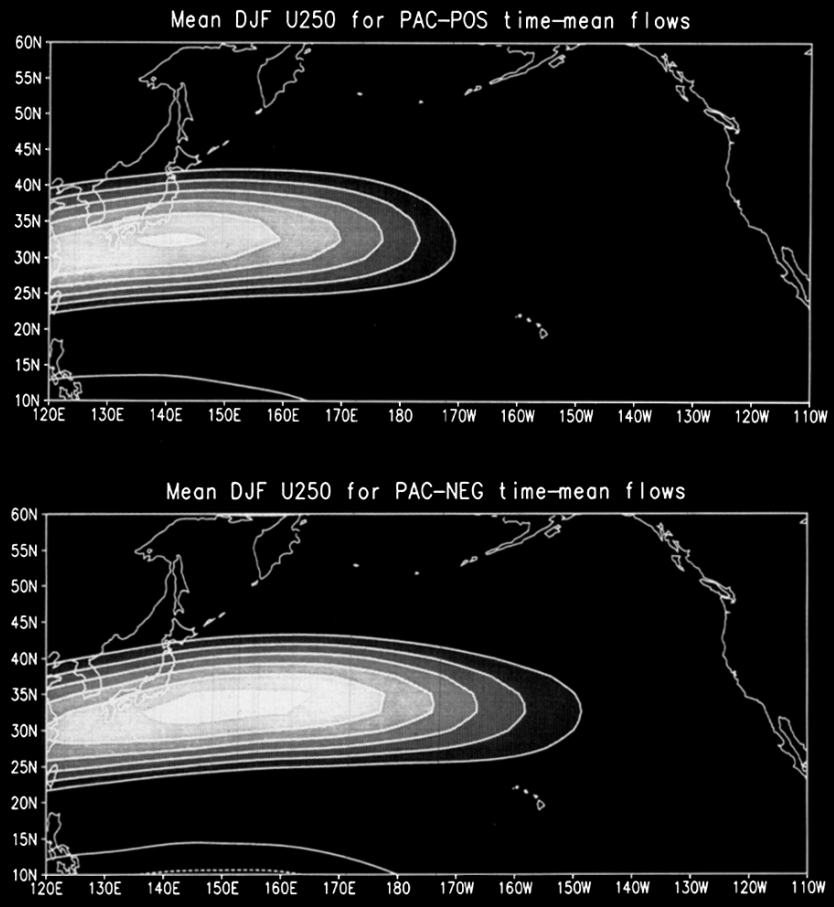

Fig. 7. The stratified DJF mean U250 for both PAC-POS and PAC-NEG time-mean flows. Contours in the shaded area start at 30 m and with interval of 5 m. The easterlies over the tropics are not shaded starting at 0 m with 5 m increment.

missing data and were not used). As shown in Fig. 10, the 31-winter LFV variances also exhibit large differences between the PAC-POS flows and the PAC-NEG flows.

5. GCM simulations

Will a general circulation model (GCM), given similar difference in basic flows, also produce large differences in LFV variance patterns? Fortunately, we have conducted some sea surface temperature (SST) impact experiments for other scientific objectives, in which there were two perpetual January GCM runs. These two experiments appear to be suitable for checking the reproducibility of the observed characteristics in LFV presented above.

Very briefly, a low resolution NMC medium-range forecast model (T40L18) (Sela, 1980; Kanamitsu, 1989; Kalnay et al., 1990) was used to run two long experiments: one with above normal tropical constant SST (SSTA run) and another with below normal tropical SST (SSTB run). The initial conditions were the same (16 January) and all boundary conditions, except SSTs, were held

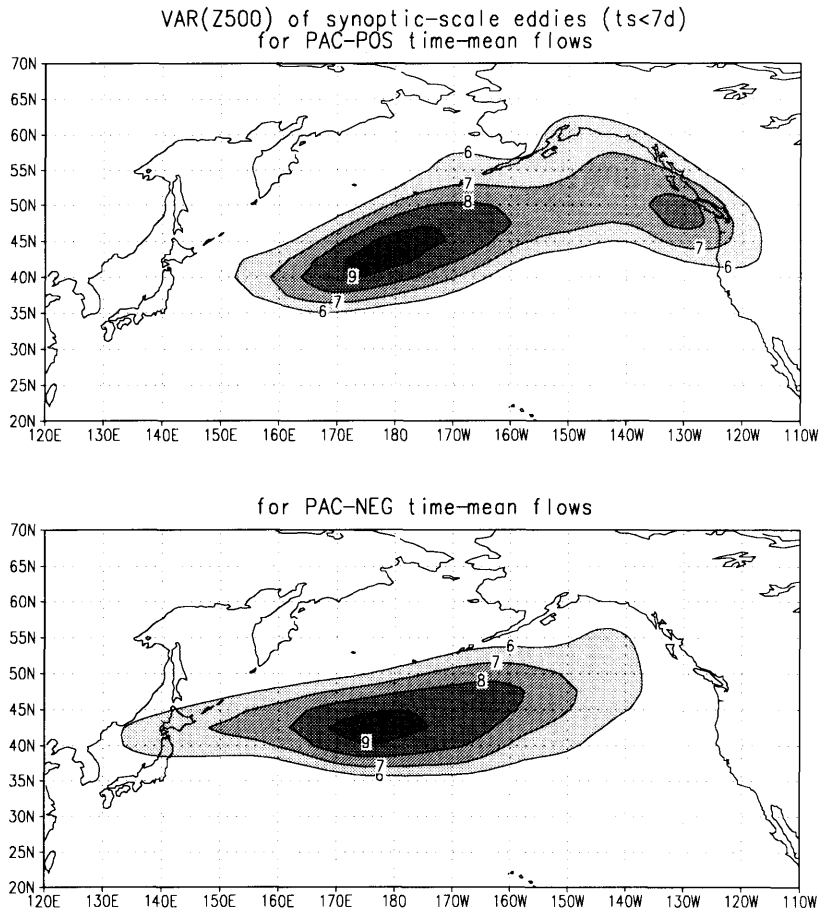

Fig. 8. The stratified Z500 variances for synoptic-scale eddies (1000 m^2).

the same for both experiments and remain fixed for 780 days of model integration. The above normal SST fields (SSTA) were the mean taken from the December 1991 and January 1992 time period, while the below normal SST fields (SSTB) were taken from the December 1988 and January 1989 time period. The difference between SSTA and SSTB is shown in Fig. 11, where a significant temperature difference of more than 4°C can be observed over the equatorial Pacific east of the date line.

The SSTA experiment simulates the El Niño boreal winter flow condition while the SSTB run simulates the La Niña flow condition. The first 50 days of model integration were discarded due to drift of the model climate. The mean Z500 difference between the SSTA and SSTB runs, as shown in the upper panel of Fig. 12, displays a very prominent PNA-like pattern, similar to the observed difference between January of 1992 and 1989, as shown in the lower panel of Fig. 12. The close resemblance gives us confidence that the SSTA and SSTB runs simulate the El Niño and La Niña mean flow conditions fairly well in the sense that they generate the impact on the mean flow in the right direction.

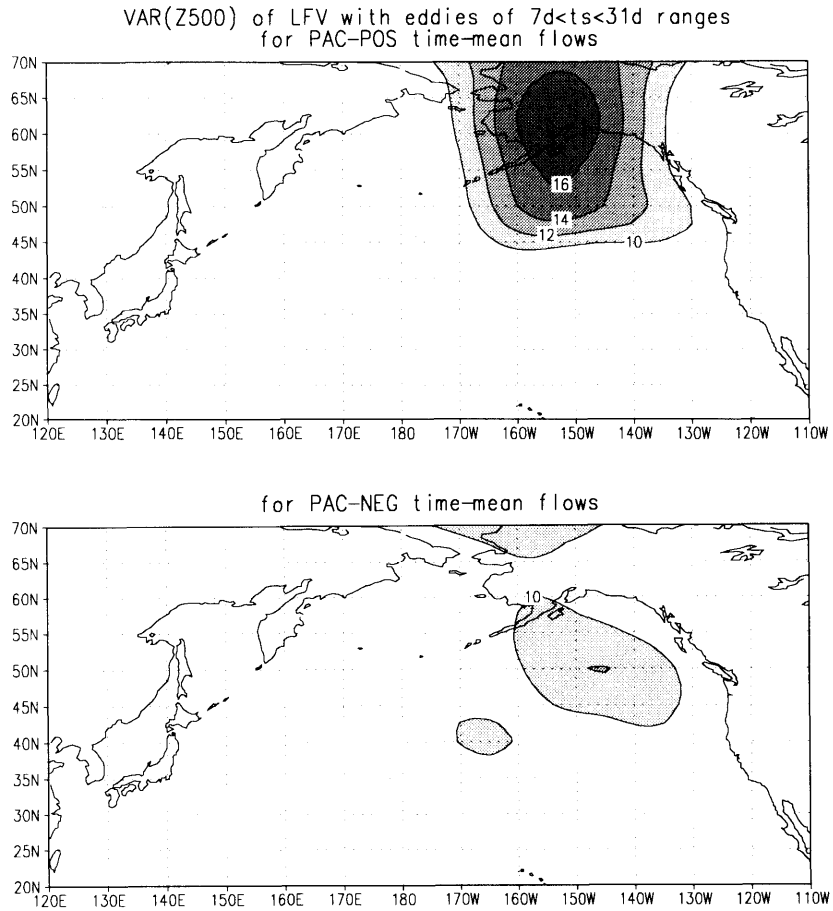

Fig. 9. The stratified Z500 variances for the LFV disturbances (1000 m^2).

The upper level westerly flows (U200) and the Z500 LFV variances were evaluated for SSTA and SSTB experiments separately. As shown in Fig. 13, the SSTA run displays strengthening and eastward extension of the jet. In Fig. 14, the LFV variance of the SSTB run is seen to be much much larger than that of the SSTA run, $(120\ m)^2$ versus $(90\ m)^2$.

From the above results (i.e., the 8-winter data, the 31-year historical data, and the GCM simulated data), a significantly large difference in LFV variance between PAC-POS and PAC-NEG flow appears to be a real phenomenon: the PAC-POS basic flows produce much larger LFV than the PAC-NEG basic flows. Again, this large difference can not be accounted for by the barotropic decay of the synoptic eddies alone, since the synoptic-scale eddy variance under the PAC-POS flow conditions is not larger than that under the PAC-NEG flow conditions, as shown in Fig. 8 for the primary data set. Other additional dynamical processes must also be operating accounting for the large difference.

Simmons et al. (1983) suggests that much of the LFV of the Northern Hemisphere wintertime general circulation is associated with disturbances which derive their energy from the basic state

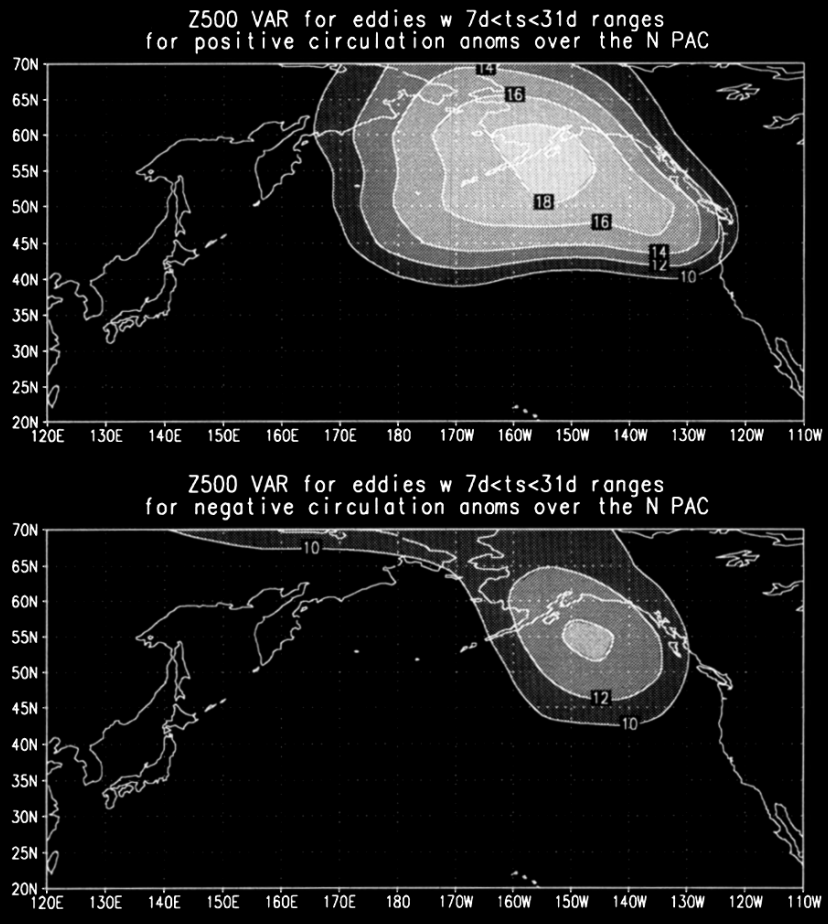

Fig. 10. Same as Fig. 9 except for being evaluated from the 34-year NMC historical Z500 data set.

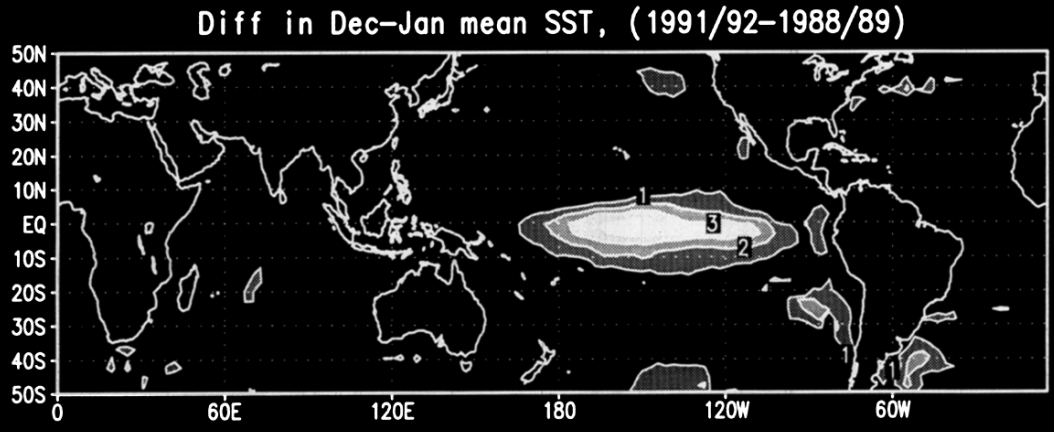

Fig. 11. The December–January mean difference in sea-surface temperature (°C).

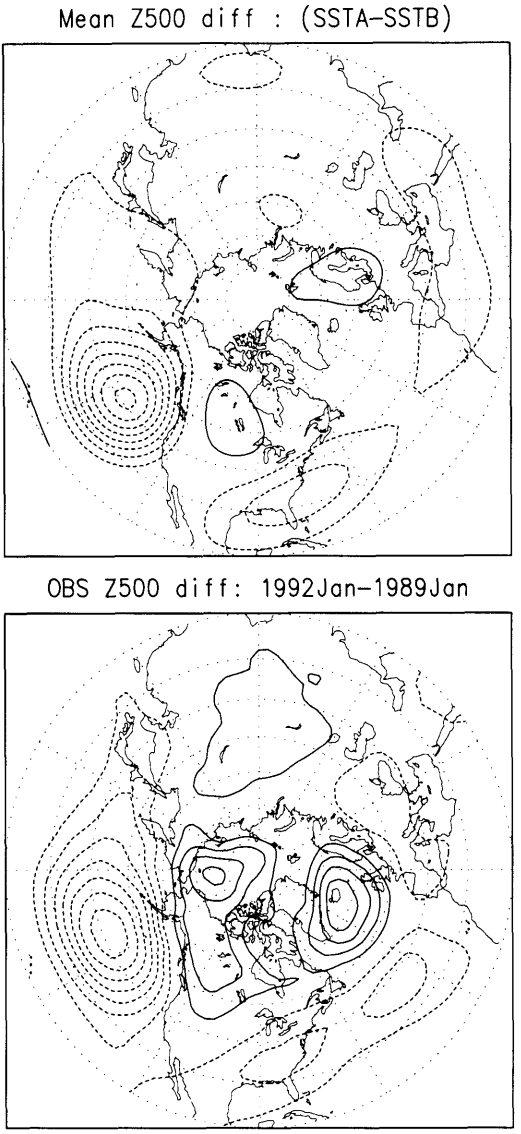

Fig. 12. Upper panel, the difference in 730-day mean Z500 between SSTA and SSTB runs. Solid (dashed) curves for positive (negative) difference. Contour starts at 20 m with 20 m increment. Lower panel, the observed difference in January-mean Z500 between 1992 (El Niño January) and 1989 (La Niña January). Note that contour starts at 40 m with 40 m increment.

through barotropic instability. Palmer (1988) suggested further that the barotropic instability of the PNA mode explains the asymmetric nature of the response of general circulation models to SST anomalies of opposite sign. It is plausible then, that the local barotropic energy conversion between the zonally varying time-mean flows and the low frequency components considered here might help to account for the large differences in the LFV variance.

6. Local perturbation energy calculation

The dynamical mechanism of large-scale instability is investigated next by examining the energy equation of a barotropic system to help account for the distinct LFV behavior presented above. Using the notations and definitions of Mak and Cai (1989), the growth rate of the local perturbation energy is governed by the scalar product, $\boldsymbol{E} \cdot \boldsymbol{D}$, in the following equation:

$$\varepsilon_t = -\boldsymbol{V} \cdot \nabla \varepsilon + \boldsymbol{E} \cdot \boldsymbol{D} - 2r\varepsilon - \boldsymbol{v} \cdot \nabla p, \tag{1}$$

where

$$\varepsilon = \tfrac{1}{2}(u^2 + v^2), \qquad \boldsymbol{v} = (u, v), \qquad \boldsymbol{V} = (U, V),$$

$$\boldsymbol{E} = (\tfrac{1}{2}(v^2 - u^2), -uv), \tag{2}$$

$$\boldsymbol{D} = (U_x - V_y, V_x + U_y). \tag{3}$$

The mean-flow advection of the perturbation energy and the ageostrophic pressure work do not contribute to the change of the global energetics, but redistribute the perturbation energy and determine the location and localization of the disturbances as discussed by Mak and Cai (1989). The $\boldsymbol{E}$-vector quantifies the local structure and the strength of the transient eddies while the $\boldsymbol{D}$-vector defines the deformation field of the time-mean flow in which the eddies are embedded.

To evaluate the barotropic energy conversion between the time-mean flow and the LFV components, we treated the disturbances with timescales between 7 and 31 days as the LFV components and the 61-day low-pass filtered Z500 as the time-mean flow. The $\boldsymbol{E}$-vector was calculated through (2) and the $\boldsymbol{D}$-vector through (3) by using finite difference method. Wind fields at 250 mb level were used.

The average inner product $\boldsymbol{E} \cdot \boldsymbol{D}$ for the entire period, DJF 1987–1994, is shown in Fig. 15. Near

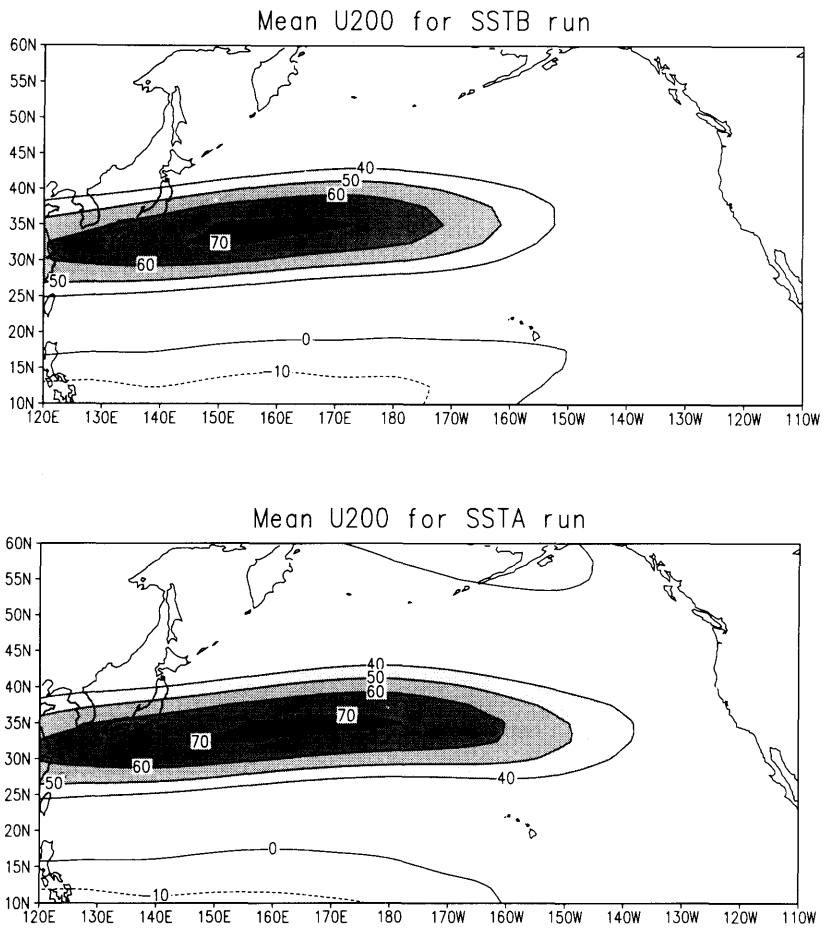

Fig. 13. The 730-day mean U200 for SSTA and SSTB runs. Solid (dashed) curves for westerly (easterly) flows.

the end of the upper westerly jet, around (32.5° N, 170° W), the generation of the LFV energy from the time-mean flow appears to be a dominant feature. Over the eastern North Pacific, however, the energy conversion is, on average, from the LFV perturbation energy to the time-mean flow.

When separate calculations were conducted for the PAC-POS and PAC-NEG time-mean flows, a large distinction was then observed, as shown in Fig. 16, where the 8-winter mean of the $\boldsymbol{E} \cdot \boldsymbol{D}$ has been subtracted before the presentation. Over the eastern North Pacific, for the PAC-NEG deformation conditions, the energy conversion is slightly more decaying of the LFV eddies into the time-mean flows (middle panel), while for the PAC-POS deformation conditions, the LFV eddies tend to still extract some energy from the time-mean flows, resulting in much larger magnitude of LFV variance (upper panel). The difference of $\boldsymbol{E} \cdot \boldsymbol{D}$ between PAC-POS and PAC-NEG (lower panel) shows clearly that, over the eastern North pacific, the extraction of the perturbation energy from the time-mean flow is much greater for the PAC-POS flows than the PAC-NEG flows.

Therefore, while the barotropic decaying of the synoptic-scale eddies into the LFV alone is not sufficient to account for the large difference in the LFV variance, the barotropic energy con-

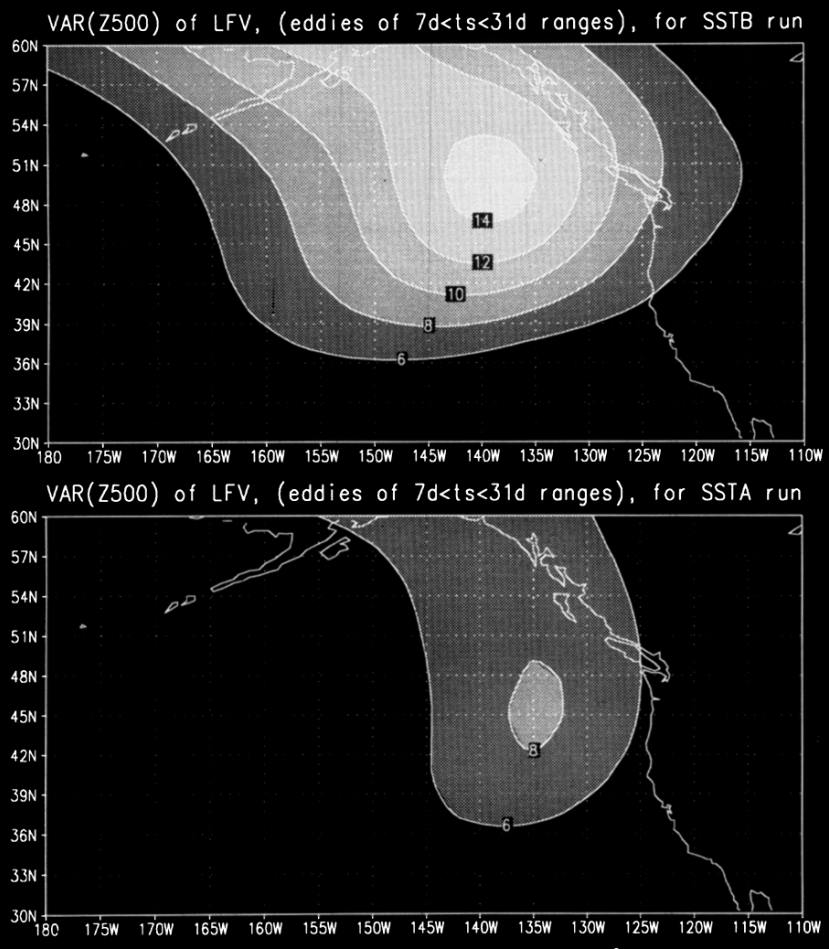

Fig. 14. The Z500 variance for the LFV disturbances of the GCM runs (1000 m^2).

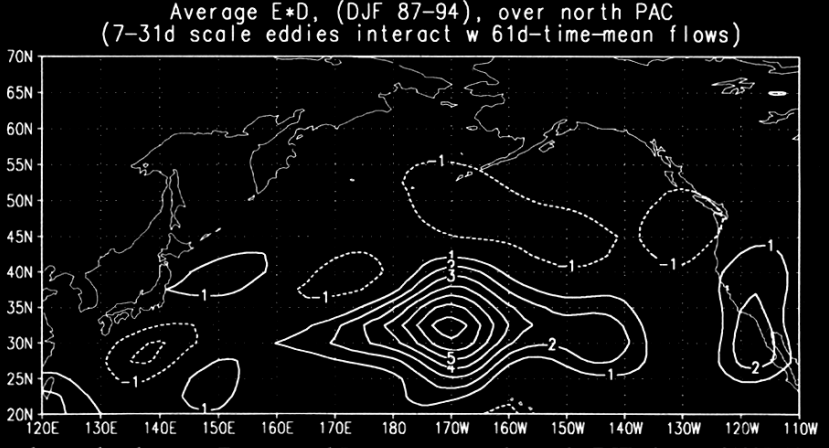

Fig. 15. The scalar product between ***E***-vector and ***D***-vector, averaged over the DJF winters of 1987–1994. Mean fields were represented by 61-day low-pass filtered time-mean flows and fluctuating components by disturbances with 7- to 31-day timescale eddies (1000^{-1} m^2/s^3). See text for details.

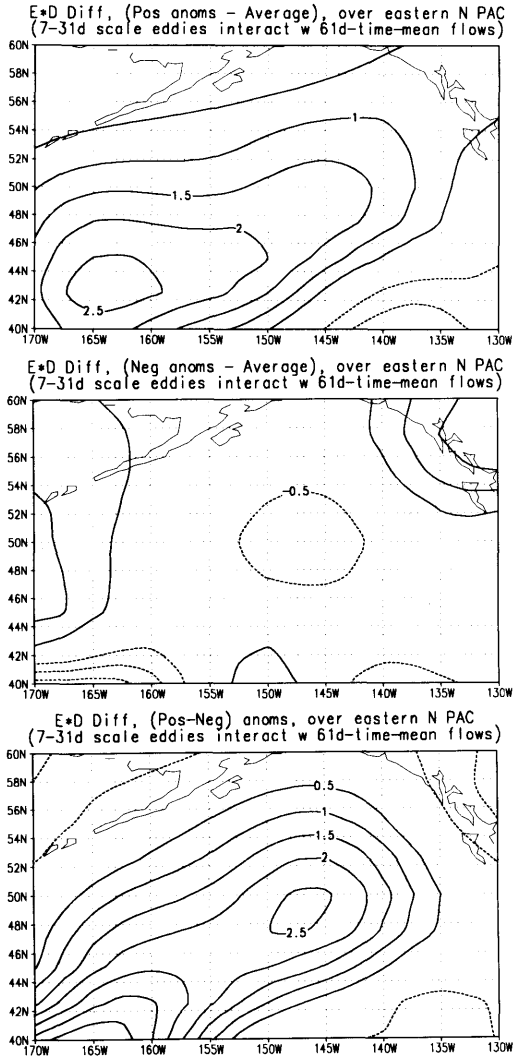

Fig. 16. The stratified $\boldsymbol{E} \cdot \boldsymbol{D}$ with the mean value (as shown in Fig. 15) subtracted. The upper two panels show the anomalies. The bottom panel shows the net difference between PAC-POS and PAC-NEG stratified flows (1000^{-1} m^2/s^3).

version between the time-mean flows and the LFV disturbances do help in accounting for the large differences shown in Fig. 9.

7. Concluding remarks

The implication of the above results is worthy of exploring. In this article, we are mainly concerned with the problem of potential predictability of the monthly means. When dealing with monthly means as a boundary value prediction problem, the internal variabilities with timescales less than 31 days necessarily become noise (Leith, 1973), operating against the signal that may be contained in the monthly means. The internal dynamics associated LFVs investigated here are the primary components of the climate noise of monthly means (Madden, 1976; Chervin, 1986; Trenberth, 1984; Jones, 1975). Therefore, a PAC-POS time-mean flow is deemed to yield relatively lower skill for a monthly mean prediction due to its inherent characteristics of much larger internal LFV being generated. Given a zonally-varying basic flow then, its large-scale barotropic instability essentially determines the extent of its low-frequency internal dynamic variabilities, as documented in this study and the works of Simmons et al. (1983) and Palmer (1988). The configuration of a basic flow can therefore be a harbinger of the potential predictability of the given flow.

Furthermore, since an anomalously warm tropical Pacific SST can force the extratropical atmosphere to assume a PAC-NEG type of time-mean flow, the warm SST anomaly can be expected to have a positive impact on the extratropical atmospheric long-range prediction in the sense that it produces smaller internal dynamics associated low frequency variabilities. On the other hand, the cold SST anomaly of an ENSO episode will exert a negative impact because of generation of large low-frequency internal dynamics variabilities. The present investigation therefore suggests a dynamical link between the phase of an ENSO episode and the potential predictability of monthly or seasonal means in the extratropical atmosphere over the North Pacific and its teleconnected areas.

Similar investigation for the north Atlantic sector is underway. The preliminary results indicate a similar behavior: much larger LFVs for the ATL-POS time-mean flows, and the barotropic decay of the synoptic-scale storms alone is not sufficient to account for this large difference. However, the close association between the tropical lower boundary forcing and the extratropical time-mean flow, that has been well observed for the north Pacific, has not been found yet for the north Atlantic sector. We plan to conduct much more detailed examinations for this important sector.

REFERENCES

Barnston, A. G. and Livezey, R. E. 1987. Classification, seasonality and persistence of low-frequency atmospheric circulation patterns. *Mon. Wea. Rev.* **115**, 1083–1126.

Blackmon, M. L. 1976. A climatological spectral study of the 500 mb geopotential height of the Northern Hemisphere. *J. Atmos. Sci.* **33**, 1607–1623.

Cai, M. and Van den Dool, H. M. 1994. Dynamical decomposition of low-frequency tendencies. *J. Atmos. Sci.* **51**, 2086–2100.

Chen, W. Y. and Van den Dool, H. M. 1995. Low-frequency anomalies in the NMC MRF model and reality. *J. of Climate* **8**, 1369–1385.

Chervin, R. M. 1986. Interannual variability and seasonal climate predictability. *J. Atmos. Sci.* **43**, 233–251.

Jones, R. H. 1975. Estimating the variance of time-averages. *J. Appl. Meteorol.* **14**, 159–163.

Kalnay, E., Kanamitsu, M. and Baker, W. E. 1990. The NMC global forecast system. *Bull. Amer. Meteorol. Soc.* **71**, 1410–1428.

Kanamitsu, M. 1989. Description of the NMC global data assimilation and forecast system. *Weather and Forecasting* **4**, 335–342.

Lau, N.-C., White, G. H. and Jenne, R. L. 1981. Circulation statistics for the extratropical Northern Hemisphere based on NMC analyses. NCAR Tech. Note 171-STR, 138 pp.

Leith, C. E. 1973. The standard error of time-average estimates of climatic means. *J. Appl. Meteorol.* **12**, 1066–1069.

Madden, R. A. 1976. Estimates of the natural variability of time-averaged sea-level pressure. *Mon. Wea. Rev.* **104**, 942–952.

Mak, Mankin and Cai, Ming 1989. Local barotropic instability. *J. Atmos. Sci.* **46**, 3289–3311.

Palmer, T. N. 1988. Medium and extended range predictability and stability of the Pacific/North American mode. *Q. J. R. Meteorol. Soc.* **114**, 691–713.

Sela, J. G. 1980. Spectral modeling at the National Meteorological Center. *Mon. Wea. Rev.* **108**, 1279–1292.

Simmons, A. J., Wallace, J. M. and Branstator, G. W. 1983. Barotropic wave propagation and instability, and atmospheric teleconnections. *J. Atmos. Sci.* **40**, 1363–1392.

Trenberth, K. E. 1984. Some effects of finite sample size and persistence on meteorological statistics. Part II: Potential predictability. *Mon. Wea. Rev.* **112**, 2369–2379.

Wallace, J. M. 1983. The climatological mean stationary waves: observational evidence. *Large-scale dynamical processes in the atmosphere*. B. J. Hoskins and R. P. Pearce, eds. Academic Press, 55–94.

Wallace, J. M. and Blackmon, M. L. 1983. Observation of low-frequency atmospheric variability. *Large-scale dynamical processes in the atmosphere*. B. J. Hoskins and R. P. Pearce, eds. Academic Press, 55–94.

Wallace, J. M. and Gutzler, D. S. 1981. Teleconnections in the geopotential height field during the Northern Hemisphere winter. *Mon. Wea. Rev.* **109**, 785–812.